# Unidirectional Magnetoresistance in Antiferromagnet/Heavy-Metal Bilayers

Soho Shim<sup>®</sup>, <sup>1,2</sup> M. Mehraeen<sup>®</sup>, <sup>3</sup> Joseph Sklenar, <sup>4,1,2</sup> Junseok Oh<sup>®</sup>, <sup>1,2</sup> Jonathan Gibbons<sup>®</sup>, <sup>1,2,5,6</sup> Hilal Saglam, <sup>5,7</sup> Axel Hoffmann<sup>®</sup>, <sup>8,5,2,1</sup> Steven S.-L. Zhang<sup>®</sup>, <sup>3</sup> and Nadya Mason<sup>®</sup>, <sup>1,2,\*</sup> <sup>1</sup>Department of Physics, University of Illinois at Urbana-Champaign, Urbana, Illinois 61801, USA <sup>2</sup>Materials Research Laboratory, University of Illinois at Urbana-Champaign, Urbana, Illinois 61801, USA

<sup>3</sup>Department of Physics, Case Western Reserve University, Cleveland, Ohio 44106, USA <sup>4</sup>Department of Physics and Astronomy, Wayne State University, Detroit, Michigan 48201, USA Materials Science Division, Argonne National Laboratory, Lemont, Illinois 60439, USA <sup>6</sup>Department of Physics, University of California San Diego, La Jolla, California 92093, USA Department of Applied Physics, Yale University, New Haven, Connecticut 06511, USA <sup>8</sup>Department of Materials Science and Engineering, University of Illinois at Urbana-Champaign, Urbana, Illinois 61801, USA



(Received 25 August 2021; revised 29 April 2022; accepted 26 May 2022; published 30 June 2022)

The interplay between electronic transport and antiferromagnetic order has attracted a surge of interest as recent studies show that a moderate change in the spin orientation of a collinear antiferromagnet may have a significant effect on the electronic band structure. Among numerous electrical probes to read out such a magnetic order, unidirectional magnetoresistance (UMR), where the resistance changes under the reversal of the current direction, can provide rich insights into the transport properties of spin-orbit-coupled systems. However, UMR has never been observed in antiferromagnets before, given the absence of intrinsic spin-dependent scattering. Here, we report a UMR in the antiferromagnetic phase of a FeRh/Pt bilayer, which undergoes a sign change and then increases strongly with an increasing external magnetic field, in contrast to UMRs in ferromagnetic and nonmagnetic systems. We show that Rashba spin-orbit coupling alone cannot explain the sizable UMR in the antiferromagnetic bilayer and that field-induced spin canting distorts the Fermi contours to greatly enhance the UMR by 2 orders of magnitude. Our results can motivate the growing field of antiferromagnetic spintronics and suggest a route to the development of tunable antiferromagnet-based spintronics devices.

DOI: 10.1103/PhysRevX.12.021069 Subject Areas: Condensed Matter Physics, Magnetism, Spintronics

#### I. INTRODUCTION

Antiferromagnets—a broad class of magnetically ordered materials—possess a variety of appealing properties [1–3] including sublattice degrees of freedom, terahertz resonance, and the lack of stray field, of which their ferromagnetic counterparts are naturally devoid. Recently, the interplay between electronic transport and the Néel order of metallic antiferromagnets has attracted a surge of interest, partly stimulated by the realization of electric control of sublattice magnetization utilizing strong spin-orbit coupling (SOC) and space-inversion symmetry breaking in collinear antiferromagnetic metals [4–9]. A moderate change in the spin

Published by the American Physical Society under the terms of the Creative Commons Attribution 4.0 International license. Further distribution of this work must maintain attribution to the author(s) and the published article's title, journal citation, and DOI.

orientation of a collinear antiferromagnet (such as spin canting) may have a significant effect on the electronic band structure and subsequently manifest itself in transport properties [10–14]. There have also been reviving efforts to develop new optical [15,16] or electrical [17-19] probes to read out antiferromagnetic order. Among these efforts, two types of linear-response magnetoresistances are commonly used in transport measurements: the anisotropic magnetoresistance in metallic antiferromagnets [4,17,18,20] and spin Hall magnetoresistance in bilayers consisting of an insulating antiferromagnet and a heavy metal [19,21–23], both of which have analogs in ferromagnetic systems [24,25].

In recent years, a new member of the family of magnetoresistances—now known as unidirectional magnetoresistance (UMR)—has been identified in various ferromagnetic heterostructures having structural inversion asymmetry [26–35]. As opposed to the aforementioned linear-response magnetoresistances, which are current independent, the UMR is linearly proportional to the applied current and changes sign when either the direction of the current or the

nadya@illinois.edu

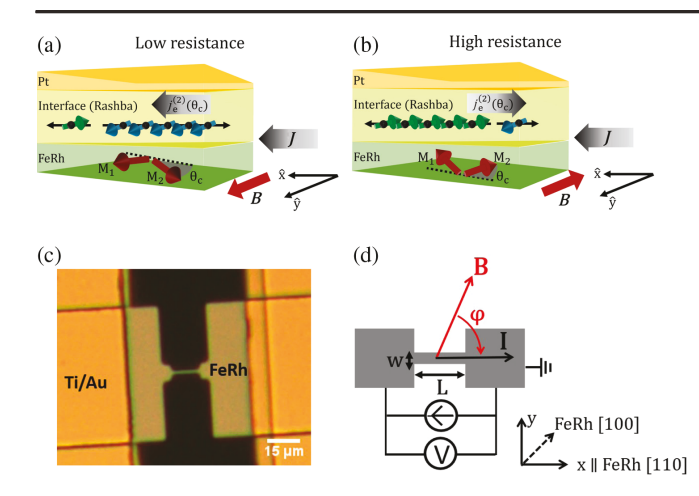


FIG. 1. UMR effect in canted antiferromagnet and sample layout. (a),(b) Rashba-effect-induced nonlinear charge current  $\mathbf{j}_e^{(2)}(\theta_c)$  at the antiferromagnet/heavy-metal interface for  $\mathbf{J} \| \hat{\mathbf{x}} \| \mathbf{J} \| - \hat{\mathbf{x}} \|$  at large field  $\mathbf{B}$ . The green and blue arrows in (a) and (b) indicate the direction of the spin polarizations. Resistance is low (high) when  $\mathbf{j}_e^{(2)}(\theta_c)$  is aligned (antialigned) with  $\mathbf{J}$ . (c) Optical microscope image of a FeRh/Pt microwire device. (d) Schematic of the longitudinal resistance measurements. A large dc current of the order of  $10^7$  A/cm<sup>2</sup> is applied to induce a UMR, while a small ac current is applied to perform the lock-in amplifier measurement. The angle  $\varphi$  is defined as the clockwise angle from the field  $\mathbf{B}$  to current  $\mathbf{I}$ , where  $\mathbf{I} = I\hat{\mathbf{x}}$ .

in-plane magnetization (which needs to be aligned perpendicularly to the current) is reversed. The analogous effect in antiferromagnetic layered structures, however, has not been explored. It is of particular interest to discover a mechanism that generates this effect in antiferromagnetic metals, given the absence of intrinsic spin-dependent scattering [36]—a key ingredient in creating the UMR effect in conducting ferromagnets [27,37].

In this work, we examine the nonlinear magnetotransport in a FeRh/Pt bilayer system. It is known that FeRh is a magnetic metal, which undergoes a metamagnetic transition near room temperature from a ferromagnetic to an antiferromagnetic phase [17,38–45]. When an in-plane magnetic field is applied perpendicularly to the current direction, a UMR is observed in the antiferromagnetic phase, which changes sign when one switches either the current or the magnetic field orientation. Furthermore, the UMR evolves nonlinearly with the external magnetic field and undergoes a sign change as the magnetic field is increased, in stark contrast to the behavior typically observed in nonmagnetic [46-50] and ferromagnetic [26,29–35] materials. We attribute the UMR effect to the combined actions of the Rashba SOC at the FeRh/Pt interface and the antiferromagnetic spin canting, as illustrated in Figs. 1(a) and 1(b). In what follows, we first present our main experimental results and then compare them to theoretical calculations of the UMR effect based on a tightbinding model Hamiltonian that encapsulates both interfacial Rashba SOC and the spin-canting effect, demonstrating excellent agreement between theory and experiment.

### II. SAMPLE LAYOUT AND TRANSPORT MEASUREMENT

We perform magnetotransport measurements on a FeRh (15 nm)/Pt (5 nm) bilayer, where the FeRh current path is oriented along the [110] direction, using lithographically defined microwires (length  $L=11~\mu\text{m}$ , width  $w=1.4~\mu\text{m}$ ), as shown in Figs. 1(c) and 1(d).

We apply a dc charge current and measure the longitudinal resistances with an additional small ac charge current of  $10 \mu A$  from a lock-in amplifier, under the application of an external magnetic field **B**. The direction of the **B** field is determined by its azimuthal angle  $\varphi$  as shown in Fig. 1(d). We can assume that the Néel order in the FeRh is aligned perpendicular to the in-plane magnetic field and smoothly rotates with it, as a result of having antiferromagnetic domains large enough to be able to define a single antiferromagnetic spin axis on average [17] and a small in-plane anisotropy which corresponds to an effective field of less than 1 T [45,51]. We note that this method allows for the UMR to be extracted with the first-harmonic output of the lockin amplifier, and that without a dc current bias, the UMR must be measured using the second-harmonic output of the lock-in amplifier [47]. As shown in Fig. 2(b), a resistance which is odd under the current polarity, defined as  $R_{\text{odd}} = [R(I) - R(-I)]/2 = -R_{\text{odd,max}} \sin \varphi$ , manifests in the first-harmonic measurement on top of the linear-response magnetoresistance background (see Supplemental Material Sec. S2 [52]). This odd resistance appears only for  $J > 10^6 \text{ A/cm}^2$ .

All the measurements are carried out at the base temperature of either 10 K (antiferromagnetic phase) or 310 K (ferromagnetic phase) [Fig. 2(a)]. Base temperature refers to the ambient temperature in the sample space. The increase in the device temperature due to Joule heating from the applied current is estimated to be about 4.35 K for  $J=10^6$  A/cm² by comparing the longitudinal resistance value under finite current density with the corresponding temperature value in Fig. 2(a). Even with the Joule heating present at a base temperature of 10 K, our device remains strictly within the antiferromagnetic phase (see Supplemental Material Sec. S1 [52]).

In Figs. 2(c) and 2(d), we show the dependence of  $R_{\rm odd,max}$  in the ferromagnetic phase on the applied current and magnetic field and observe a monotonic increase with respect to the applied current.  $R_{\rm odd,max}$  in the ferromagnetic phase can be fitted with the curve  $\alpha J + \beta J^3$  [Fig. 2(c)], which includes the contributions from spin-dependent and magnon-scattering mechanisms, in agreement with previous reports on UMR generated in ferromagnetic-metal/normal-metal bilayers [34]. Furthermore, we observe a suppression in  $R_{\rm odd,max}$  for fields above 1 T, scaling with the

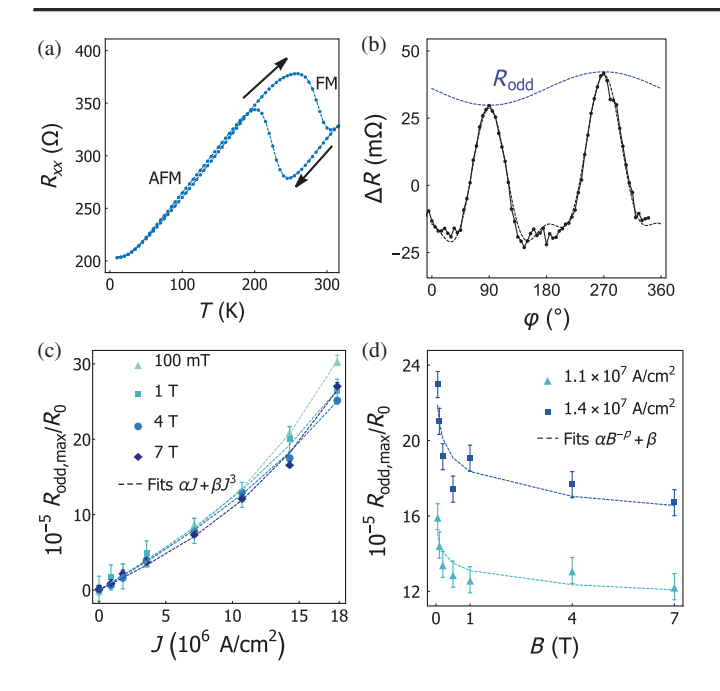


FIG. 2. Magnetoresistance characterization and UMR in the ferromagnetic phase of FeRh/Pt. (a) Temperature sweep of the longitudinal resistance under an external in-plane field of B=4 T. Clear transition between the ferromagnetic (FM) phase and the antiferromagnetic (AFM) phase is observed. (b) Angular sweep at T=10 K (AFM phase) and B=4 T, under  $J=1.43\times 10^7$  A/cm².  $\Delta R$  is defined as  $\Delta R=R-R_{\rm av}$ . A magnetoresistance which is odd under the current polarity  $R_{\rm odd}$  manifests under high current density. (c)  $R_{\rm odd,max}$  in the FM phase of FeRh [110]/Pt as a function of J at various field magnitudes.  $R_{\rm odd,max}$  is normalized with the base resistance  $R_0$  (measured at J=0 and B=0). Dashed lines show the fitting curves  $\alpha J+\beta J^3$ . (d)  $R_{\rm odd,max}$  in the FM phase of FeRh [110]/Pt as a function of J at various current densities J. Dashed lines show the fitting curves  $\alpha B^{-p}+\beta J^{-p}$ .

power law  $B^{-p}$  [Fig. 2(d)]. This amplitude suppression is also consistent with previous studies of UMR in ferromagnetic-metal/normal-metal bilayers [34], where the UMR originates from the field-induced gap in the magnon excitation spectrum, which reduces the electron-magnon scattering at high fields.

# III. OBSERVATION OF UMR IN AN ANTIFERROMAGNET

The behavior of the UMR in the antiferromagnetic phase is shown in Figs. 3(a) and 3(b). In order to extract the UMR from  $R_{\rm odd}$  in the antiferromagnetic phase, we analyze the contribution from the thermal gradient  $\nabla T$  and related thermoelectric effects. The anomalous Nernst effect and spin Seebeck effect, both producing a longitudinal voltage proportional to  $\mathbf{M} \times \nabla T$  (where  $\mathbf{M}$  is the net magnetization and  $\nabla T \propto J^2$ ), can give rise to the same angular dependence as observed for the UMR when  $\nabla T \| \hat{\mathbf{z}} \| [26,53,54]$ . Here, by measuring the transverse (Hall) counterpart scaled

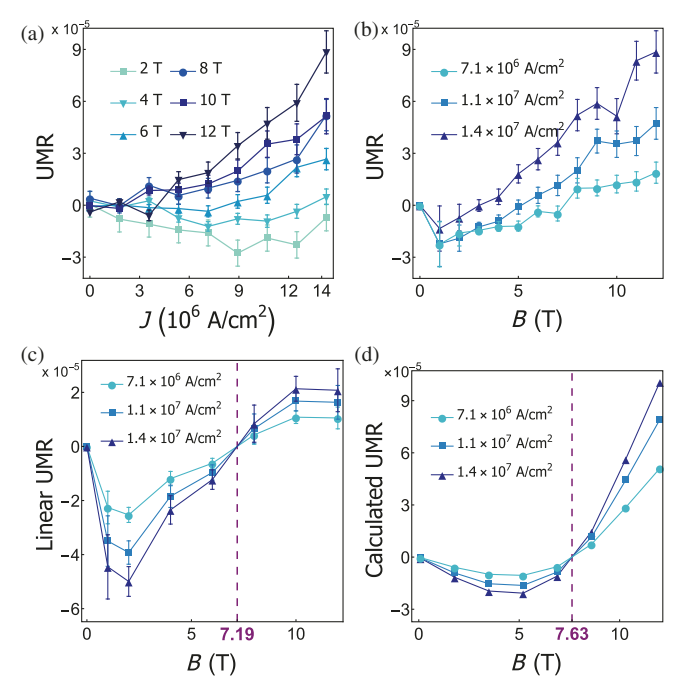


FIG. 3. UMR in the antiferromagnetic phase of FeRh/Pt. (a) UMR in the antiferromagnetic phase of FeRh [110]/Pt as a function of J for various field magnitudes. (b) UMR in the antiferromagnetic phase of FeRh [110]/Pt as a function of field B at various current densities J. (c) Extracted linear UMR with respect to the field B, with the purple dashed line indicating the observed field value at which the UMR undergoes a sign change. The observed sign-change field value is  $7.19 \pm 0.17 \, \mathrm{T}$  (see Supplemental Material Sec. S8 [52]). (d) Calculated UMR in the antiferromagnetic phase as a function of B for different values of the applied current, with the purple dashed line indicating the theoretically predicted field value at which the UMR undergoes a sign change. Parameters used:  $a = 3 \text{ Å}, \tau = 10^{-14} \text{ s}, g = 2$ ,  $\epsilon_0 = 10 \text{ eV}, \quad \epsilon_F = 0.617\epsilon_0, \quad t = 0.1\epsilon_0 \quad [55], \quad \Delta_{\text{ex}} = 0.05\epsilon_0$ [55,56],  $\tilde{\alpha}_R = \alpha_R/a = 0.05\epsilon_0$  [55,57],  $H_J = 11.83$  T (corresponding to  $\theta_c = 25^{\circ}$  at B = 10 T), and width of spectral function =  $0.002\epsilon_0$ .

by the geometric factor L/w in a similar FeRh/Pt microwire device, we find that even the maximum thermoelectric voltage contribution in the antiferromagnetic phase is less than 30% (see Supplemental Material Sec. S3 [52]). We also find that  $R_{\text{odd,max}}$ , the amplitude of  $R_{\text{odd}}$ , has no dependence on current or external field strength in a control sample of FeRh (20 nm) without Pt (see Supplemental Material Sec. S3 [52]), which indicates a negligible anomalous Nernst effect contribution, in agreement with the literature. We conclude that there is an additional magnetoresistance effect in the FeRh/Pt bilayers other than thermoelectric voltages. For the antiferromagnetic phase of the FeRh/Pt bilayer, we extract the UMR from the amplitude of the measured sinusoidal signal [shown in Fig. 2(b)] using UMR  $\sin \varphi = -(R_{\text{odd}} - R_{xx}^{\nabla T})/R_0$ , following the convention for ferromagnetic-metal/normal-metal bilayers, in which the UMR of the bilayer increases when the direction of the majority spins in the ferromagnet and the spin accumulation vector are parallel to each other, and decreases when they are antiparallel [26].

In the antiferromagnetic phase of the FeRh/Pt bilayer [Figs. 3(a) and 3(b)], we observe a different trend from what was observed in the ferromagnetic phase. In the antiferromagnetic phase, the UMR is not strongly suppressed for fields higher than 1 T. This can be attributed to the lack of magnon-dependent scattering in antiferromagnets [36]. Thus, the antiferromagnetic UMR increases approximately linearly with field and current, for large field and current values. The most striking feature of the UMR in the antiferromagnetic phase is the sign change from negative to positive UMR as the magnetic field is increased, which, to our knowledge, has not been observed in either ferromagnetic or nonmagnetic systems.

The UMR observed in the antiferromagnetic phase cannot be due to the spin Hall effect, since the scattering in a metallic antiferromagnet is independent of the spin polarization [36] and even the canted spin configuration under the external field is not large enough to induce the necessary spindependent scattering for a significant spin Hall UMR (see Supplemental Material Sec. S7 [52]). Moreover, the observed UMR is isotropic with respect to the direction of the current flow in the crystalline plane (see Supplemental Material Sec. S4 [52]). Thus, it is unlikely that the UMR in the antiferromagnetic phase originates from strong crystal field effects. A lack of field and current dependence of  $R_{\rm odd,max}$  in the control sample of FeRh (20 nm) without a Pt layer (see Supplemental Material Sec. S3 [52]) also implies that the observed UMR cannot be attributed to the intrinsic properties of FeRh.

As we discuss in the next section, we attribute the UMR in FeRh/Pt to the combined effects of the Rashba SOC at the interface of FeRh and Pt, and the spin canting in the antiferromagnetic spin sublattices. A calculated UMR based on this theory, which is linear in the applied current, is shown in Fig. 3(d); this can be compared to the linear component of the experimental UMR (i.e., to first order in the applied current) shown in Fig. 3(c). As can be seen, in the intermediate magnetic field range—where the UMR sign reversal occurs—there is excellent qualitative and quantitative agreement between theory and experiment. In the low-field limit, however, there is some quantitative disagreement. This is most likely attributable to the effect of thermal magnons, which was not considered in the theoretical model. As an additional scattering source of conduction electrons, the thermal magnons may modify the magnetoresistance at low magnetic fields, but their contribution is expected to diminish as the external field is increased—a trend which is nicely captured by comparing Figs. 3(c) and 3(d).

# IV. PHYSICAL ORIGIN OF UMR

To obtain physical insight into the observed UMR effect arising from the FeRh/Pt interface, we theoretically

investigate the nonlinear magnetotransport by restricting ourselves to the interfacial layer of the FeRh adjacent to the Pt layer, which may be described by the following two-dimensional tight-binding Hamiltonian with broken inversion symmetry of a collinear antiferromagnetic metal with Rashba SOC [2,55]

$$\hat{H} = \epsilon_0 + \gamma_{\mathbf{k}} \hat{\tau}_x + \Delta_{\mathbf{e}x} \hat{\tau}_z \hat{\boldsymbol{\sigma}} \cdot \mathbf{m} + \alpha_R \hat{\tau}_x \hat{\boldsymbol{\sigma}} \cdot \hat{\mathbf{z}} \times \mathbf{k} + g\mu_B \hat{\boldsymbol{\sigma}} \cdot \mathbf{B},$$
(1)

where  $\epsilon_0$  is the on-site energy,  $\Delta_{\rm ex}$  is the s-d exchange constant between the local moments and the electron,  $\alpha_R$  is the Rashba SOC constant, and  $\hat{\tau}_i$  and  $\hat{\sigma}_i$  are Pauli matrices which signify the sublattice and spin degrees of freedom, respectively. The nearest-neighbor hopping is represented by  $\gamma_{\bf k} = -2t(\cos k_x a + \cos k_y a)$ , where t is the hopping term and a the lattice constant.

In the absence of an external magnetic field, the Rashba splitting leads to two Fermi contours with opposite spin chirality in equilibrium, as shown in Fig. 4(a). By applying an in-plane electric field **E**, a pure nonlinear spin current (with no corresponding charge current) can be induced in the system due to spin-momentum locking as well as the symmetric electron distribution in momentum space in the second order of the **E** field [50,58,59]. The nonlinear spin current is converted to a nonlinear charge current in the presence of an in-plane magnetic field perpendicular to the current direction [which establishes an imbalance between the two electron fluxes with opposite spin orientations; see dashed bands in Fig. 4(b)], leading to the UMR effect [50,59].

The Hamiltonian given by Eq. (1) is modified by spin canting when an external magnetic field is applied perpendicular to the Néel vector. More specifically, the sublattice magnetizations tilt toward the applied field by an angle  $\theta_c$  relative to the Néel vector, resulting in a net magnetization along the field direction. The canting angle  $\theta_c$  can be determined by minimizing the magnetic energy density of a collinear antiferromagnet as given below

$$\epsilon_m = -\mathbf{B} \cdot (\mathbf{M}_A + \mathbf{M}_B) + \frac{H_J}{M_A} \mathbf{M}_A \cdot \mathbf{M}_B. \tag{2}$$

Here,  $\mathbf{M}_A$  and  $\mathbf{M}_B$  are the magnetizations of sublattices A and B,  $H_J$  is the effective exchange field measuring the interaction between the two sublattices, and  $M_s$  is the saturation magnetization, where we take  $M_A = M_B = M_s$ . For an external magnetic field applied along the y direction, we find  $\theta_c = \arcsin{(B/2H_J)}$  (see Supplemental Material Sec. S5 [52]). To capture the spin-canting effect, we make the substitution  $\Delta_{\rm ex}\hat{\tau}_z\hat{\sigma}_x \to \Delta_{\rm ex}(\hat{\tau}_z\hat{\sigma}_x\cos\theta_c+\hat{\sigma}_y\sin\theta_c)$  for the s-d exchange term in the Hamiltonian. Note that the net magnetization that is parallel to  $\mathbf{B}$  now couples with the same sign to the electronic spin, giving rise to an effective magnetic field  $B_{sd} = \Delta_{\rm ex}B/(2g\mu_B H_J)$ .

This strong effective magnetic field due to spin canting greatly enhances the amount of distortion of the Fermi

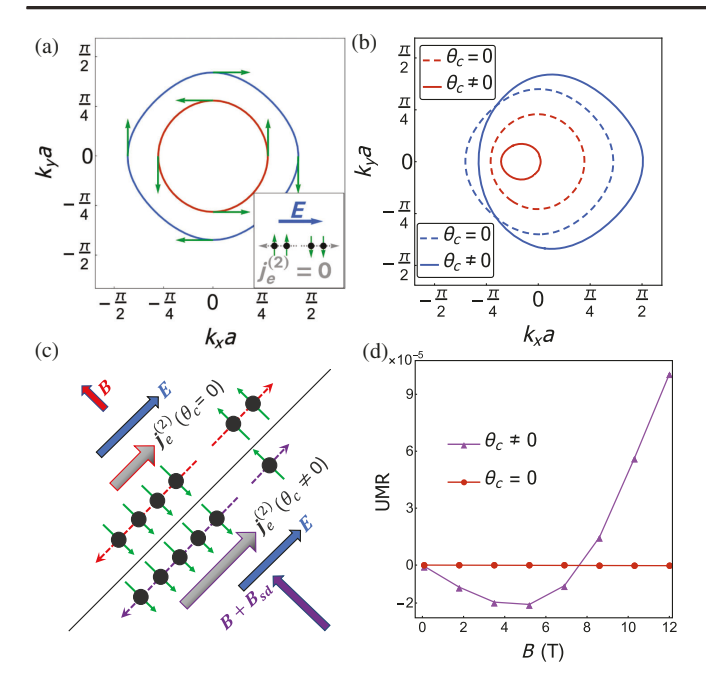


FIG. 4. Enhancement of UMR by spin canting. (a) Spin texture of the conduction bands in the absence of a magnetic field. Because of spin-momentum locking arising from the Rashba effect, when an electric field is applied, a pure spin current but no nonlinear charge current is produced, as depicted in the inset. (b) Spin-dependent distortion of the bands in the presence of a magnetic field at both zero canting (dashed curves) and finite canting (solid curves). The two bands are shown here in red and blue. (c) Generation of a nonlinear charge current transverse to the applied **B** field (top left), which increases considerably in the presence of canting (bottom right). (d) Plots of the calculated UMR at finite and vanishing canting as functions of the magnetic field *B*. In the presence of canting, the UMR is stronger by 2 orders of magnitude.

contours when an external magnetic field is applied, as shown by the solid bands in Fig. 4(b), which leads to a more profound UMR, as shown schematically in Fig. 4(c). To confirm this qualitative understanding, we calculate the nonlinear longitudinal charge-current density  $j_{e,x}^{(2)} = -(e^3\tau^2E_x^2/\hbar^2)\sum_n\int_{\bf k}\left(\partial^2f_n/\partial k_x^2\right)v_{n,x}$  using the Boltzmann transport formalism (see Supplemental Material Sec. S5 [52]), where n is the band index,  $\tau$  is the momentum relaxation time,  $\int_{\bf k}\equiv\int_{\rm BZ}[d^2{\bf k}/(2\pi)^2]$ , and  ${\bf v}_n\!=\!\partial\epsilon_n({\bf k})/\hbar\partial{\bf k}$  is the group velocity of the nth band. From the total longitudinal resistivity  $\rho_{xx}=E_x/j_{e,x}$ , we calculate the UMR as UMR  $\equiv$   $-[\rho_{xx}(E_x)-\rho_{xx}(-E_x)]/\rho_{xx}(E_x)\approx 2\sigma_{xx}^{(1)}/\sigma_D$ , with  $\sigma_{xx}^{(1)}=j_{e,x}^{(2)}/E_x$  and  $\sigma_D$  the Drude conductivity. The calculated UMR, both with and without canting, as a function of the applied magnetic field is plotted in Fig. 4(d), from which it is evident that spin canting indeed plays an important role in the enhancement of the UMR effect.

# V. MECHANISM OF UMR SIGN CHANGE

In order to understand the origin of the sign change in the UMR as the magnetic field intensity is tuned, we first note

that this is made possible by spin canting. More precisely, in the presence of canting, the Hamiltonian acquires a significant nonlinear dependence on the magnetic field through the effective field  $B_{sd}$ , which, in turn, allows for the UMR to evolve nonlinearly with respect to B. Another element that plays an important role is the asymmetry of the band structure as the magnetic field and, by extension,  $B_{sd}$ , are switched on.

Initially, at zero magnetic field, as depicted in Fig. 5(a), the conduction bands are symmetric about the  $\Gamma$  point and the UMR is absent. When the magnetic field is turned on, a small spin-dependent asymmetry develops in the band structure, which results in a positive UMR contribution from the outer band (blue in Fig. 5) and a negative contribution from the inner band (red). As shown in Figs. 5(b) and 5(d), at low fields such as 3 T, the asymmetry in the outer band is not enough to counter the dominant presence of the inner band near the Fermi level and the overall UMR is negative.

As the magnetic field strength is increased, the inner band continues its ascent from the Fermi sea, while the asymmetry of the outer band near the Fermi level continues to grow. At around 7–8 T, the contribution of the two bands becomes equal, at which point the overall UMR undergoes a sign change. As depicted in Fig. 5(c), at large fields, the contribution from the outer band is dominant near the

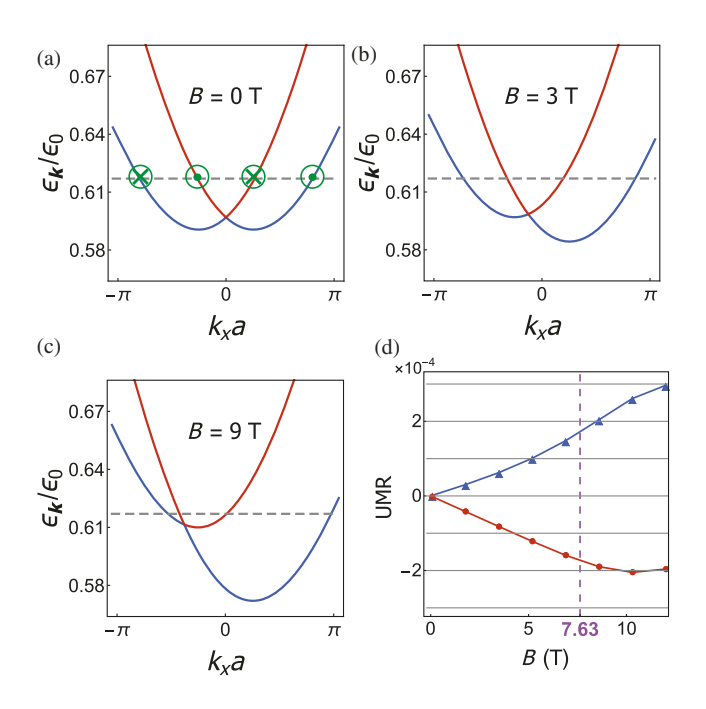


FIG. 5. Mechanism of UMR sign change. Structure of the conduction bands at  $k_y = 0$  and (a) 0 T, (b) 3 T, and (c) 9 T, indicating the breaking of time-reversal symmetry induced by the magnetic field. The two bands are shown here in red and blue, with the dashed line indicating the Fermi level. (d) Opposite contributions of the inner (red dots) and outer (blue triangles) conduction bands to the UMR, with the purple dashed line indicating the field at which the sign change in the overall UMR occurs.

Fermi level and the UMR is positive. The dependence of the UMR for each conduction band on the magnetic field for a given current value is displayed in Fig. 5(d), along with the theoretically predicted field value of 7.63 T at which the sign change occurs. This value may be compared with the sign-change field of the linear components of the observed UMR [Fig. 3(c)]. The observed magnetic field value of  $7.19 \pm 0.17$  T is in very good agreement with the theoretically predicted field value.

Based on this picture, it is also possible to understand why such a magnetic-field-dependent sign change in the UMR is unique to antiferromagnetic systems and is not expected to occur in ferromagnetic and nonmagnetic systems. In the latter, one could still have a positive or negative UMR depending on the relative position of the Fermi level with respect to the conduction bands; however, the UMR would not change sign in these systems due to the lack of sublattice degrees of freedom and the resulting antiferromagnetic spin canting (see Supplemental Material Sec. S6 [52]).

#### VI. CONCLUSION

In summary, we observe a UMR in the antiferromagnetic phase of a FeRh/Pt bilayer, which undergoes a sign change and then increases strongly with an increasing external magnetic field, largely different from UMRs in ferromagnetic and nonmagnetic systems. We show that the Rashba SOC alone, a mechanism known for UMRs in ferromagnetic and nonmagnetic systems, cannot explain the sizable UMR in the antiferromagnetic bilayer. Antiferromagnetic spin canting also plays a crucial role in enhancing the UMR by inducing a strong effective magnetic field that significantly distorts the band structure.

The UMR effect we observe is not exclusive to FeRh/Pt bilayers and is expected to exist in antiferromagnetic heterostructures satisfying two conditions: an easy-plane antiferromagnet which displays magnetic domains large enough to define a single antiferromagnetic spin axis on average, and small in-plane anisotropy to ensure coherent rotation of the spin axis with an applied in-plane field. Thus, in the context of antiferromagnetism, this effect has both fundamental and practical implications. First, the new mechanism for UMR in the antiferromagnetic bilayer can advance fundamental understanding of noncollinear antiferromagnetic systems. Antiferromagnets have recently attracted great interest as systems that host emergent phenomena, competing orders, and symmetry-tunable band structures. Therefore, our findings can motivate future studies to further explore the interplay between spin texture, electronic band structure, and the associated emergent phenomena in antiferromagnets.

Moreover, the key parameters of antiferromagnets (difficult to measure in thin films) can be back-engineered from the UMR effect. For example, susceptibility and magnetocrystalline anisotropy parameters have not been directly measured in FeRh thin films [45]. Based on the field

dependence of the UMR that we report, we can estimate the magnetic susceptibility of the 15-nm-thick FeRh thin films to be 5 times greater than what has been reported for bulk samples (see Supplemental Material Sec. S5 [52]). In addition, our analysis reveals that while the value of the UMR sign-reversal field is, in general, a complicated function of the materials parameters of the bilayer system, we expect that it will scale linearly with the magnetic susceptibility (see Supplemental Material Sec. S9 [52])— a prediction which may prove useful in future studies of UMR in other antiferromagnetic systems. From the perspective of applications, our findings may also lead to the development of antiferromagnet-based spintronics, such as two-terminal devices [60,61], where the spin information can be controlled by both electric voltage and magnetic field.

#### ACKNOWLEDGMENTS

We thank David G. Cahill and Matthew J. Gilbert for valuable discussions. This research is primarily supported by the NSF through the University of Illinois at Urbana-Champaign Materials Research Science and Engineering Center Grant No. DMR-1720633 and is carried out in part in the Materials Research Laboratory Central Research Facilities, University of Illinois. Thin-film growth was supported as part of Quantum Materials for Energy Efficient Neuromorphic Computing (Q-MEEN-C), an Energy Frontier Research Center funded by the U.S. Department of Energy (DOE), Office of Science, Basic Energy Sciences (BES), under Award No. DE-SC0019273. J.O. acknowledges support from the U.S. Army under Grant No. W911NF-20-1-0024. Work by M.M. and S. S.-L. Z. is supported by the College of Arts and Sciences, Case Western Reserve University.

S. S. and M. M. contributed equally to this work. S. S., J. S., and N. M. designed the magnetotransport experiments. J. G., H. S., and A. H. were responsible for synthesizing FeRh films. S. S. and J. S. performed magnetic characterization of FeRh. S. S., J. S., J. O., J. G., and H. S. fabricated devices. S. S., J. S., and J. O. performed magnetotransport experiments. A. H. and N. M. supervised the experimental work. M. M. and S. S.-L. Z. devised the theory. S. S. and M. M. analyzed the results with J. S., S. S.-L. Z., and N. M. providing input. S. S., M. M., J. S., S. S.-L. Z., and N. M. wrote the manuscript with input from all other authors.

#### APPENDIX: MATERIALS AND METHODS

The FeRh films used in this work are deposited onto (100) MgO substrates using dc magnetron sputtering. Before sputtering, the substrates are annealed within the sputter deposition system at 850 °C for one hour in order to desorb the potential contaminants on the surface. After the substrates are cleaned, the temperature is lowered to 450 °C for deposition. The sputter target used for deposition is an

equiatomic FeRh source. During growth, 6.5 sccm of Ar gas is introduced into the chamber, and the pressure is set to 6 mTorr. The dc sputtering power used is 50 W, and the growth rate is 0.7 Å/s. After one-hour postannealing of FeRh films at 650 °C, the heater is turned off and the films are cooled down to room temperature before depositing the Pt layer, which is deposited at room temperature, with the pressure of 5 mTorr, power of 7 W, and the growth rate of 0.6 Å/s [62]. The films are subsequently patterned into microwires by direct-writing laser lithography and Ar milling. The microwires are patterned so that the current flows along the [110] crystalline orientations of FeRh.

For thin FeRh films deposited onto MgO substrates, it has been reported that there exist residual ferromagnetic moments confined to within 6-8 nm of the interface of FeRh and MgO [63]. To determine the magnitude of the residual ferromagnetic moment, magnetic characterization on FeRh (15 nm) with an in-plane field is carried out in a vibrating sample magnetometer by Quantum Design. With an in-plane field of 0.5 T, the residual ferromagnetic moment at T = 10 K is estimated to be 4% of the saturated magnetization in the ferromagnetic phase (1260 emu/cm<sup>3</sup>) (see Supplemental Material Sec. S10 [52]). The residual ferromagnetic moment, however, does not affect the UMR because no UMR is observed for the single-layer FeRh thin film on MgO (see Supplemental Material Sec. S3 [52]), and the field scale for the observed antiferromagnetic UMR is very large compared to the ferromagnetic case (see Figs. 2 and 3). Transport experiments are four-probe resistance measurements carried out using the Physical Property Measurement System by Quantum Design equipped with a horizontal rotator module. A dc current of the order of mA, generated by a Keithley source meter 2400, is applied to achieve the desired current density J, and a 13-Hz ac current of 10 µA generated by a Stanford Research Systems SR830 lock-in amplifier is applied to probe the magnetoresistance. To accommodate different device sizes, the current is adapted to have the same current density. The rotation of the sample is provided by a motorized stage with a precision of 0.0133°.

- [1] T. Jungwirth, X. Marti, P. Wadley, and J. Wunderlich, *Antiferromagnetic Spintronics*, Nat. Nanotechnol. **11**, 231 (2016).
- [2] V. Baltz, A. Manchon, M. Tsoi, T. Moriyama, T. Ono, and Y. Tserkovnyak, *Antiferromagnetic Spintronics*, Rev. Mod. Phys. 90, 015005 (2018).
- [3] S. A. Siddiqui, J. Sklenar, K. Kang, M. J. Gilbert, A. Schleife, N. Mason, and A. Hoffmann, *Metallic Antiferromagnets*, J. Appl. Phys. 128, 040904 (2020).
- [4] P. Wadley, B. Howells, J. Železný, C. Andrews, V. Hills, R. P. Campion, V. Novák, K. Olejník, F. Maccherozzi, S. S. Dhesi et al., Electrical Switching of an Antiferromagnet, Science 351, 587 (2016).

- [5] S. Y. Bodnar, L. Šmejkal, I. Turek, T. Jungwirth, O. Gomonay, J. Sinova, A. Sapozhnik, H.-J. Elmers, M. Kläui, and M. Jourdan, Writing and Reading Antiferromagnetic Mn<sub>2</sub>Au by Néel Spin-Orbit Torques and Large Anisotropic Magnetoresistance, Nat. Commun. 9, 348 (2018).
- [6] P. Wadley, S. Reimers, M. J. Grzybowski, C. Andrews, M. Wang, J. S. Chauhan, B. L. Gallagher, R. P. Campion, K. W. Edmonds, S. S. Dhesi et al., Current Polarity-Dependent Manipulation of Antiferromagnetic Domains, Nat. Nanotechnol. 13, 362 (2018).
- [7] M. Meinert, D. Graulich, and T. Matalla-Wagner, *Electrical Switching of Antiferromagnetic* Mn<sub>2</sub>Au *and the Role of Thermal Activation*, Phys. Rev. Applied **9**, 064040 (2018).
- [8] X. F. Zhou, J. Zhang, F. Li, X. Z. Chen, G. Y. Shi, Y. Z. Tan, Y. D. Gu, M. S. Saleem, H. Q. Wu, F. Pan, and C. Song, Strong Orientation-Dependent Spin-Orbit Torque in Thin Films of the Antiferromagnet Mn<sub>2</sub>Au, Phys. Rev. Applied 9, 054028 (2018).
- [9] S. DuttaGupta, A. Kurenkov, O. A. Tretiakov, G. Krishnaswamy, G. Sala, V. Krizakova, F. Maccherozzi, S. Dhesi, P. Gambardella, S. Fukami et al., Spin-Orbit Torque Switching of an Antiferromagnetic Metallic Heterostructure, Nat. Commun. 11, 5715 (2020).
- [10] T. Suzuki, R. Chisnell, A. Devarakonda, Y. T. Liu, W. Feng, D. Xiao, J. W. Lynn, and J. G. Checkelsky, *Large Anomalous Hall Effect in a Half-Heusler Antiferromagnet*, Nat. Phys. 12, 1119 (2016).
- [11] K. S. Takahashi, H. Ishizuka, T. Murata, Q. Y. Wang, Y. Tokura, N. Nagaosa, and M. Kawasaki, *Anomalous Hall Effect Derived from Multiple Weyl Nodes in High-Mobility* EuTiO<sub>3</sub> *Films*, Sci. Adv. 4 (2018).
- [12] X. Li, A. H. MacDonald, and H. Chen, *Quantum Anomalous Hall Effect through Canted Antiferromagnetism*, arXiv:1902.10650.
- [13] R. Yang, M. Corasaniti, C. C. Le, Z. Y. Liao, A. F. Wang, Q. Du, C. Petrovic, X. G. Qiu, J. P. Hu, and L. Degiorgi, *Spin-Canting-Induced Band Reconstruction in the Dirac Material* Ca<sub>1-x</sub>Na<sub>x</sub>MnBi<sub>2</sub>, Phys. Rev. Lett. **124**, 137201 (2020).
- [14] J. Kipp, K. Samanta, F. R. Lux, M. Merte, D. Go, J.-P. Hanke, M. Redies, F. Freimuth, S. Blügel, M. Ležaić, and Y. Mokrousov, *The Chiral Hall Effect in Canted Ferromagnets and Antiferromagnets*, Commun. Phys. **4**, 99 (2021).
- [15] A. V. Kimel, A. Kirilyuk, A. Tsvetkov, R. V. Pisarev, and T. Rasing, *Laser-Induced Ultrafast Spin Reorientation in the Antiferromagnet* TmFeO<sub>3</sub>, Nature (London) **429**, 850 (2004).
- [16] V. Saidl, P. Němec, P. Wadley, V. Hills, R. P. Campion, V. Novák, K. W. Edmonds, F. Maccherozzi, S. S. Dhesi, B. L. Gallagher et al., Optical Determination of the Néel Vector in a CuMnAs Thin-Film Antiferromagnet, Nat. Photonics 11, 91 (2017).
- [17] X. Marti, I. Fina, C. Frontera, J. Liu, P. Wadley, Q. He, R. Paull, J. Clarkson, J. Kudrnovský, I. Turek *et al.*, *Room-Temperature Antiferromagnetic Memory Resistor*, Nat. Mater. **13**, 367 (2014).
- [18] T. Moriyama, K. Oda, T. Ohkochi, M. Kimata, and T. Ono, *Spin Torque Control of Antiferromagnetic Moments in NiO*, Sci. Rep. **8**, 14167 (2018).

- [19] L. Baldrati, A. Ross, T. Niizeki, C. Schneider, R. Ramos, J. Cramer, O. Gomonay, M. Filianina, T. Savchenko, D. Heinze, A. Kleibert, E. Saitoh, J. Sinova, and M. Klaui, Full Angular Dependence of the Spin Hall and Ordinary Magnetoresistance in Epitaxial Antiferromagnetic NiO(001)/Pt Thin Films, Phys. Rev. B 98, 024422 (2018).
- [20] T. Moriyama, N. Matsuzaki, K.-J. Kim, I. Suzuki, T. Taniyama, and T. Ono, Sequential Write-Read Operations in FeRh Antiferromagnetic Memory, Appl. Phys. Lett. 107, 122403 (2015).
- [21] G. R. Hoogeboom, A. Aqeel, T. Kuschel, T. T. M. Palstra, and B. J. van Wees, *Negative Spin Hall Magnetoresistance of Pt on the Bulk Easy-Plane Antiferromagnet NiO*, Appl. Phys. Lett. **111**, 052409 (2017).
- [22] J. Fischer, O. Gomonay, R. Schlitz, K. Ganzhorn, N. Vlietstra, M. Althammer, H. Huebl, M. Opel, R. Gross, S. T. B. Goennenwein, and S. Geprägs, *Spin Hall Magneto-resistance in Antiferromagnet/Heavy-Metal Heterostructures*, Phys. Rev. B 97, 014417 (2018).
- [23] A. Manchon, Spin Hall Magnetoresistance in Antiferromagnet/Normal Metal Bilayers, Phys. Status Solidi RRL 11, 1600409 (2017).
- [24] T. McGuire and R. Potter, Anisotropic Magnetoresistance in Ferromagnetic 3d Alloys, IEEE Trans. Magn. 11, 1018 (1975).
- [25] H. Nakayama, M. Althammer, Y.-T. Chen, K. Uchida, Y. Kajiwara, D. Kikuchi, T. Ohtani, S. Geprägs, M. Opel, S. Takahashi, R. Gross, G. E. W. Bauer, S. T. B. Goennenwein, and E. Saitoh, *Spin Hall Magnetoresistance Induced by a Nonequilibrium Proximity Effect*, Phys. Rev. Lett. 110, 206601 (2013).
- [26] C. O. Avci, K. Garello, A. Ghosh, M. Gabureac, S. F. Alvarado, and P. Gambardella, *Unidirectional Spin Hall Magnetoresistance in Ferromagnet/Normal Metal Bilayers*, Nat. Phys. 11, 570 (2015).
- [27] S. S.-L. Zhang and G. Vignale, *Theory of Unidirectional Spin Hall Magnetoresistance in Heavy-Metal/Ferromagnetic-Metal Bilayers*, Phys. Rev. B **94**, 140411(R) (2016).
- [28] K. Yasuda, A. Tsukazaki, R. Yoshimi, K. S. Takahashi, M. Kawasaki, and Y. Tokura, *Large Unidirectional Magneto-resistance in a Magnetic Topological Insulator*, Phys. Rev. Lett. 117, 127202 (2016).
- [29] S. Langenfeld, V. Tshitoyan, Z. Fang, A. Wells, T. Moore, and A. Ferguson, *Exchange Magnon Induced Resistance Asymmetry in Permalloy Spin-Hall Oscillators*, Appl. Phys. Lett. **108**, 192402 (2016).
- [30] T. Li, S. Kim, S.-J. Lee, S.-W. Lee, T. Koyama, D. Chiba, T. Moriyama, K.-J. Lee, K.-J. Kim, and T. Ono, *Origin of Threshold Current Density for Asymmetric Magnetoresist-ance in Pt/Py Bilayers*, Appl. Phys. Express 10, 073001 (2017).
- [31] Y. Yin, D.-S. Han, M. C. de Jong, R. Lavrijsen, R. A. Duine, H. J. Swagten, and B. Koopmans, *Thickness Dependence of Unidirectional Spin-Hall Magnetoresistance in Metallic Bilayers*, Appl. Phys. Lett. **111**, 232405 (2017).
- [32] K. Olejník, V. Novák, J. Wunderlich, and T. Jungwirth, Electrical Detection of Magnetization Reversal without Auxiliary Magnets, Phys. Rev. B **91**, 180402(R) (2015).
- [33] Y. Lv, J. Kally, D. Zhang, J.S. Lee, M. Jamali, N. Samarth, and J.-P. Wang, *Unidirectional Spin-Hall and*

- Rashba-Edelstein Magnetoresistance in Topological Insulator-Ferromagnet Layer Heterostructures, Nat. Commun. 9, 111 (2018).
- [34] C. O. Avci, J. Mendil, G. S. D. Beach, and P. Gambardella, Origins of the Unidirectional Spin Hall Magnetoresistance in Metallic Bilayers, Phys. Rev. Lett. 121, 087207 (2018).
- [35] T. Guillet, A. Marty, C. Vergnaud, M. Jamet, C. Zucchetti, G. Isella, Q. Barbedienne, H. Jaffrès, N. Reyren, J. M. George, and A. Fert, Large Rashba Unidirectional Magnetoresistance in the Fe/Ge(111) Interface States, Phys. Rev. B 103, 064411 (2021).
- [36] A. S. Núñez, R. A. Duine, P. Haney, and A. H. MacDonald, Theory of Spin Torques and Giant Magnetoresistance in Antiferromagnetic Metals, Phys. Rev. B 73, 214426 (2006).
- [37] S. S.-L. Zhang and G. Vignale, Theory of Unidirectional Magnetoresistance in Magnetic Heterostructures, Proc. SPIE Int. Soc. Opt. Eng. 10357, 1035707 (2017).
- [38] J. S. Kouvel and C. C. Hartelius, Anomalous Magnetic Moments and Transformations in the Ordered Alloy FeRh, J. Appl. Phys. 33, 1343 (1962).
- [39] J.-U. Thiele, S. Maat, and E. E. Fullerton, FeRh/FePt Exchange Spring Films for Thermally Assisted Magnetic Recording Media, Appl. Phys. Lett. **82**, 2859 (2003).
- [40] R. Cherifi, V. Ivanovskaya, L. Phillips, A. Zobelli, I. Infante, E. Jacquet, V. Garcia, S. Fusil, P. Briddon, N. Guiblin et al., Electric-Field Control of Magnetic Order above Room Temperature, Nat. Mater. 13, 345 (2014).
- [41] Y. Lee, Z. Liu, J. T. Heron, J. D. Clarkson, J. Hong, C. Ko, M. D. Biegalski, U. Aschauer, S.-L. Hsu, M. E. Nowakowski et al., Large Resistivity Modulation in Mixed-Phase Metallic Systems, Nat. Commun. 6, 1 (2015).
- [42] A. Chirkova, K. Skokov, L. Schultz, N. Baranov, O. Gutfleisch, and T. Woodcock, Giant Adiabatic Temperature Change in FeRh Alloys Evidenced by Direct Measurements under Cyclic Conditions, Acta Mater. 106, 15 (2016).
- [43] J. Barker and R. W. Chantrell, *Higher-Order Exchange Interactions Leading to Metamagnetism in FeRh*, Phys. Rev. B **92**, 094402 (2015).
- [44] X. Chen, J. Feng, Z. Wang, J. Zhang, X. Zhong, C. Song, L. Jin, B. Zhang, F. Li, M. Jiang et al., Tunneling Anisotropic Magnetoresistance Driven by Magnetic Phase Transition, Nat. Commun. 8, 1 (2017).
- [45] B. R. McGrath, R. E. Camley, and K. L. Livesey, *Self-Consistent Local Mean-Field Theory for Phase Transitions and Magnetic Properties of FeRh*, Phys. Rev. B **101**, 014444 (2020).
- [46] T. Ideue, K. Hamamoto, S. Koshikawa, M. Ezawa, S. Shimizu, Y. Kaneko, Y. Tokura, N. Nagaosa, and Y. Iwasa, *Bulk Rectification Effect in a Polar Semiconductor*, Nat. Phys. 13, 578 (2017).
- [47] T. Guillet, C. Zucchetti, Q. Barbedienne, A. Marty, G. Isella, L. Cagnon, C. Vergnaud, H. Jaffrès, N. Reyren, J.-M. George, A. Fert, and M. Jamet, *Observation of Large Unidirectional Rashba Magnetoresistance in Ge(111)*, Phys. Rev. Lett. **124**, 027201 (2020).
- [48] Y. Fan, Q. Shao, L. Pan, X. Che, Q. He, G. Yin, C. Zheng, G. Yu, T. Nie, M.R. Masir *et al.*, *Unidirectional*

- Magneto-Resistance in Modulation-Doped Magnetic Topological Insulators, Nano Lett. 19, 692 (2019).
- [49] P. He, S.M. Walker, S. S.-L. Zhang, F. Y. Bruno, M. S. Bahramy, J. M. Lee, R. Ramaswamy, K. Cai, O. Heinonen, G. Vignale, F. Baumberger, and H. Yang, *Observation of Out-of-Plane Spin Texture in a* SrTiO<sub>3</sub>(111) *Two-Dimensional Electron Gas*, Phys. Rev. Lett. **120**, 266802 (2018).
- [50] P. He, S. S.-L. Zhang, D. Zhu, Y. Liu, Y. Wang, J. Yu, G. Vignale, and H. Yang, Bilinear Magnetoelectric Resistance as a Probe of Three-Dimensional Spin Texture in Topological Surface States, Nat. Phys. 14, 495 (2018).
- [51] E. Mancini, F. Pressacco, M. Haertinger, E. Fullerton, T. Suzuki, G. Woltersdorf, and C. Back, Magnetic Phase Transition in Iron–Rhodium Thin Films Probed by Ferromagnetic Resonance, J. Phys. D 46, 245302 (2013).
- [52] See Supplemental Material at http://link.aps.org/ supplemental/10.1103/PhysRevX.12.021069 for additional characterization and analysis.
- [53] M. Weiler, M. Althammer, F. D. Czeschka, H. Huebl, M. S. Wagner, M. Opel, I.-M. Imort, G. Reiss, A. Thomas, R. Gross, and S. T. B. Goennenwein, *Local Charge and Spin Currents in Magnetothermal Landscapes*, Phys. Rev. Lett. 108, 106602 (2012).
- [54] T. Kikkawa, K. Uchida, Y. Shiomi, Z. Qiu, D. Hou, D. Tian, H. Nakayama, X.-F. Jin, and E. Saitoh, *Longitudinal Spin Seebeck Effect Free from the Proximity Nernst Effect*, Phys. Rev. Lett. **110**, 067207 (2013).
- [55] J. Železný, H. Gao, K. Výborný, J. Zemen, J. Mašek, A. Manchon, J. Wunderlich, J. Sinova, and T. Jungwirth, Relativistic Néel-Order Fields Induced by Electrical Current in Antiferromagnets, Phys. Rev. Lett. 113, 157201 (2014).

- [56] H. B. M. Saidaoui, X. Waintal, and A. Manchon, Robust Spin Transfer Torque in Antiferromagnetic Tunnel Junctions, Phys. Rev. B 95, 134424 (2017).
- [57] P. M. Haney, H.-W. Lee, K.-J. Lee, A. Manchon, and M. D. Stiles, Current Induced Torques and Interfacial Spin-Orbit Coupling: Semiclassical Modeling, Phys. Rev. B 87, 174411 (2013).
- [58] K. Hamamoto, M. Ezawa, K. W. Kim, T. Morimoto, and N. Nagaosa, Nonlinear Spin Current Generation in Noncentrosymmetric Spin-Orbit Coupled Systems, Phys. Rev. B 95, 224430 (2017).
- [59] P. He, S. S.-L. Zhang, D. Zhu, S. Shi, O. G. Heinonen, G. Vignale, and H. Yang, *Nonlinear Planar Hall Effect*, Phys. Rev. Lett. 123, 016801 (2019).
- [60] I. M. Miron, K. Garello, G. Gaudin, P.-J. Zermatten, M. V. Costache, S. Auffret, S. Bandiera, B. Rodmacq, A. Schuhl, and P. Gambardella, *Perpendicular Switching of a Single Ferromagnetic Layer Induced by In-Plane Current Injection*, Nature (London) 476, 189 (2011).
- [61] L. Liu, C.-F. Pai, Y. Li, H. Tseng, D. Ralph, and R. Buhrman, *Spin-Torque Switching with the Giant Spin Hall Effect of Tantalum*, Science **336**, 555 (2012).
- [62] H. Saglam, Spin Transport and Spin-Orbit Torques in Antiferromagnets, Ph. D. thesis, Illinois Institute of Technology, 2019.
- [63] R. Fan, C. J. Kinane, T. R. Charlton, R. Dorner, M. Ali, M. A. de Vries, R. M. D. Brydson, C. H. Marrows, B. J. Hickey, D. A. Arena, B. K. Tanner, G. Nisbet, and S. Langridge, Ferromagnetism at the Interfaces of Antiferromagnetic FeRh Epilayers, Phys. Rev. B 82, 184418 (2010).